Electronic supporting information

Monocrystalline $Ni_{12}P_5$ hollow spheres with good morphology and ultrahigh specific surface area as advanced electrocatalysts for the hydrogen evolution reaction

Jinfa Chang[a,b,d], Songtao Li[c], Guoqiang Li[a,b,d], Junjie Ge[a,b,*], Changpeng Liu[a,b] and Wei Xing[a,b,*]

*Corresponding author: W. Xing, E-mail: xingwei@ciac.ac.cn

J. Ge, E-mail: gejj@ciac.ac.cn

Tel.: 86-431-85262223; Fax: 86-431-85685653

[a] State Key Laboratory of Electroanalytical Chemistry, Changchun Institute of Applied Chemistry, 5625 Renmin Street, Changchun 130022, PR China

[b] Laboratory of Advanced Power Sources, Jilin Province Key Laboratory of Low Carbon Chemical Power Sources, Changchun Institute of Applied Chemistry, 5625 Renmin Street, Changchun 130022, PR China

[c] Institute of Mathematics, Jilin University, Changchun 130012, PR China

[d] University of Chinese Academy of Sciences, Beijing 100039, PR China

Experimental Section

Materials

Sodium hypophosphite monohydrate (≥ 99.0%, $NaH_2PO_2 \cdot H_2O$), nickel sulfate hexahydrate (≥ 98.0%, $NiSO_4 \cdot 6H_2O$), Pt/C (20%) were purchased from Aldrich Chemical Co. (USA). Nafion solution (5%) was purchased from Dupont Co. (USA). CTAB, n-butanol, cyclohexane, sulfuric acid (≥ 98.0%, H_2SO_4) and ethanol (≥ 99.7%) were purchased from Beijing Chemical Co. (China). All the chemicals were of analytical grade and used as received. Highly purified N_2 was supplied by Changchun Juyang Co Ltd. Ultrapure water (resistivity：$\rho \geq 18$ MΩ cm) was used to prepare the solutions.

Physical characterizations

Scanning electron microscopy (SEM) measurements were performed with an XL 30 ESEM FEG field emission scanning electron microscope. Transmission electron microscopy (TEM), high resolution transmission electron microscopy (HR-TEM), high-annular dark-field scanning transmission electron microscopy (STEM), line-scan electron energy loss spectroscopy (EELS) and element mapping analysis were conducted on Philips TECNAI G2 electron microscope operating at 200 kV. X-ray diffraction (XRD) measurements were performed with a PW-1700 diffractometer using a Cu K_α (λ=1.5405 Å) radiation source (Philips Co.). The textural and morphological features of the $Ni_{12}P_5$ hollow spheres were determined by nitrogen physisorption at 77 K in a Micromeritics ASAP 2020. Textural properties such as the specific surface area pore volume and pore size distribution were calculated from each corresponding nitrogen adsorption−desorption isotherm, applying the Brunauer−Emmett−Teller (BET) equation and the Barrett−Joyner−Halenda (BJH). To explore the hollow structure of the $Ni_{12}P_5$ spheres, the $Ni_{12}P_5$ spheres sample with reaction times of 24 h was ball-milled with planetary ball-milling instrument for 1 hours. The bulk compositions of $Ni_{12}P_5$ hollow spheres were evaluated using an inductively coupled plasma-atomic emission spectrometer (ICP-AES, X Series 2, Thermo Scientific USA).

Electrochemical measurements

Electrochemical measurements were performed with EG & G PARSTAT 4000 potentiostat/galvanostat (Princeton Applied Research Co., USA). A conventional one-component three-electrode cell was used, including a glassy carbon electrode (GCE, geometric area = 0.07 cm^2) as the working electrode, a graphite plate was used as the auxiliary electrode and a saturated calomel electrode (SCE, Hg/Hg_2Cl_2) electrode was used as the reference electrode. To prepare the working electrode, 5 mg of the catalyst and 50 μL of 5 wt% Nafion solution were dispersed in 950 mL of ethanol solvent, followed by ultrasounded at least 30 min. Then a certain amount of the ink was dropped onto a GCE (~loading: 0.71 mg cm^{-2}). For the HER reactions, the electrolyte (0.5 M H_2SO_4) was degassed by bubbling N_2 for at least 30 minutes before the electrochemical measurements. Prior recording the HER activity of $Ni_{12}P_5$ hollow spheres, the catalysts

were activated by 20 CV scans along the potential window of 0.1 to -0.5 V vs. RHE in 0.5 M H_2SO_4 at a scan rate of 100 mV s^{-1}, then the linear sweep voltammetry (LSV) with a scan rate of 5 mV s^{-1} was performed. All the potentials reported in our work were vs. the reversible hydrogen electrode (RHE). In 0.5 M H_2SO_4 (pH = 0.56), E(RHE) = 0.242+ 0.059*pH. Ohmic drop was corrected using the current interrupt methods, all data have been corrected for 90% iR potential drop. The electrochemical impedance spectra (EIS) were recorded at the frequency range from 100 kHz to 10 mHz with 10 points per decade in 0.5 M H_2SO_4. The amplitude of the sinusoidal potential signal was 5 mV.

The generated gas was confirmed by gas chromatography analysis and measured quantitatively using a calibrated pressure sensor to monitor the pressure change in the anode compartment of a H-type electrolytic cell. The glass carbon sheet (1*2 cm) was used as working electrode with a catalysts loading of 0.536 mg cm^{-2}. The Faradaic efficiency was calculated by comparing the amount of measured hydrogen with calculated hydrogen generated at a constant oxidative current of 10 mA cm^{-2} in 0.5 M H_2SO_4 for at least 100 min electrolysis (assuming 100% FE). Pressure data during electrolysis were recorded using a CEM DT-8890 Differential Air Pressure Gauge Manometer Data Logger Meter Tester with a sampling interval of 1 point per second.

Table S1 Comparison of HER activities of $Ni_{12}P_5$ hollow spheres catalysts with recently published nickel phosphide catalysts.

Materials	Electrolytes	Scan rate (mV s^{-1})	Onset potential (mV)	Current density (j, mA cm^{-2})	Overpotential @ (mV @ cm^{-2})	Tafel slope (mV dec^{-1})	References
$Ni_{12}P_5$ hollow spheres	0.50 M H_2SO_4	5	37	10	144	46	This work
				20	173		
				50	225		
				100	277		
$Ni_{12}P_5$ solid spheres			95	10	225	59	
				20	263		
				50	324		
				100	375		
Ni_2P/Ti	0.50 M H_2SO_4	5	-	20	130	46	[1]
				100	180		
Ni_2P	1 M H_2SO_4	5	50	20	140	66	[2]
	1 M KOH			20	250	102	
$Ni_{12}P_5$/Ti	0.50 M H_2SO_4	5	-	10	107	63	[3]
				20	143±3		
NiP_2 NS/CC	0.50 M H_2SO_4	2	50	10	75	51	[4]
				100	204		
	1 M KOH		74	10	102	65	
				100	270		
tungsten-doped Ni_2P microspheres	0.50 M H_2SO_4	5	50	20	110	39	[5]
				100	180		
Ni_2P/Ti	1 M H_2SO_4	2	60	20	138	60	[6]
				100	188		

Ni_2P@graphitized carbon fiber	0.50 M H_2SO_4	5	45	10	54	46	[7]
				100	135		
peapod like Ni_2P/C	0.50 M H_2SO_4	5	60	10	87	54	[8]
				20	115		
Ni_2P-G/NF	0.50 M H_2SO_4	5	50	10	75	51	[9]
				20	160		
Fe-doped Ni_2P	0.50 M H_2SO_4	5	~50	50	150	45	[10]
Ni_2P-G/NF	0.50 M H_2SO_4	5	0	10	55	~30	[11]
	1 M KPi	5	0	5	50	~40	
	1 M KOH	5	7	100	200	32	
AlNiP-TT	1 M KOH	5	16	10	111	65	[12]
				20	142		
Ni_5P_4	1 M H_2SO_4	1	-	10	23	33	[13]
				100	32		
	1 M KOH			10	49	98	
				100	202		
Ni_2P nanorods	0.1 M KOH	5	200	30	500	-	[14]
Ni_2P	0.50 M H_2SO_4	5	-	100	240	75	[15]
Ni_2P/CNT	0.50 M H_2SO_4	5	88	10	124	53	[16]

Fig. S1 The enlarged SEM (a), HR-TEM (b) images and SA-XRD (c) of $Ni_{12}P_5$ hollow spheres.

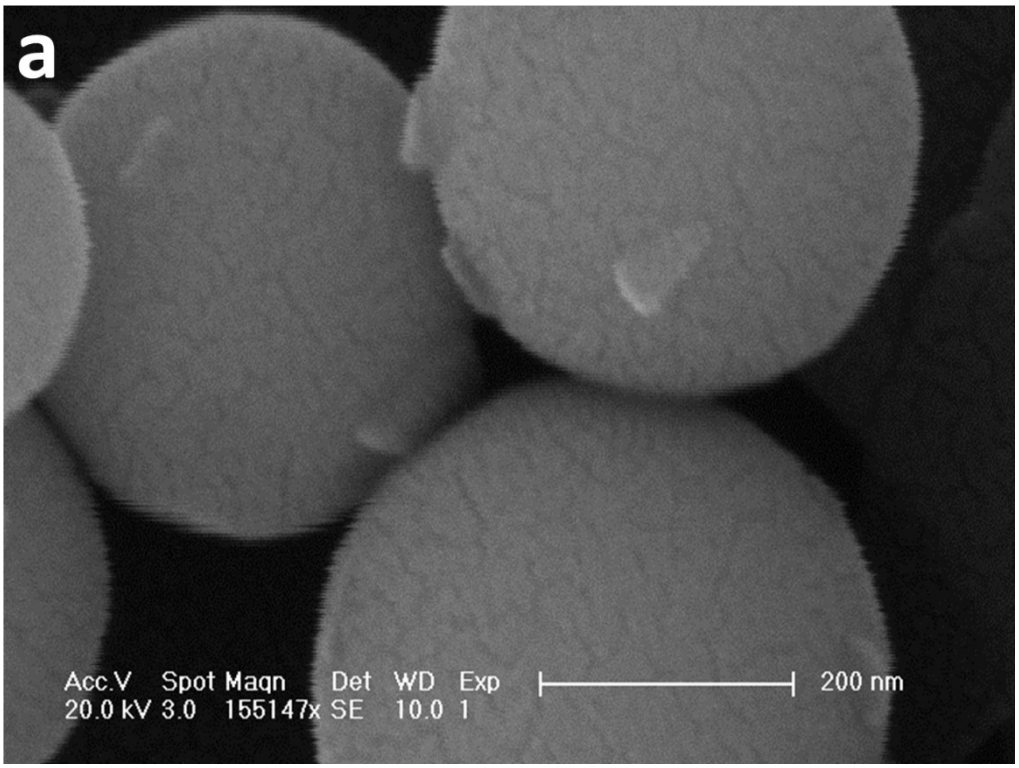

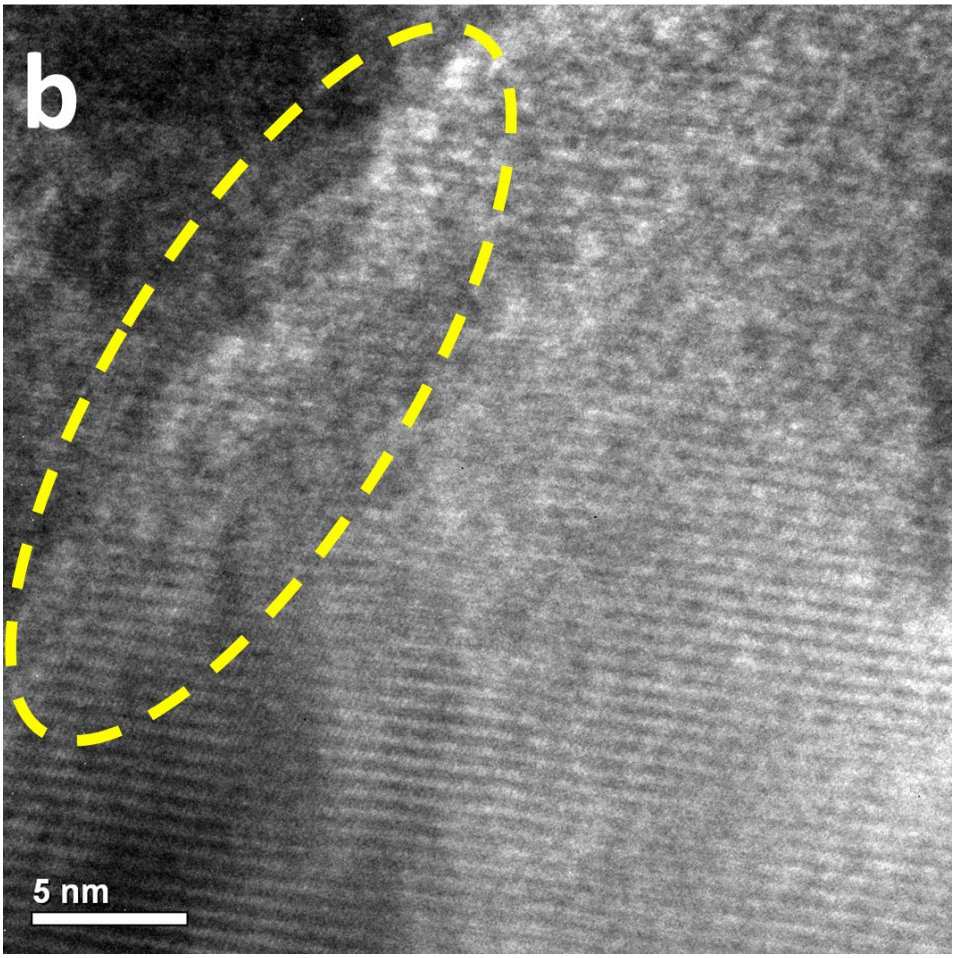

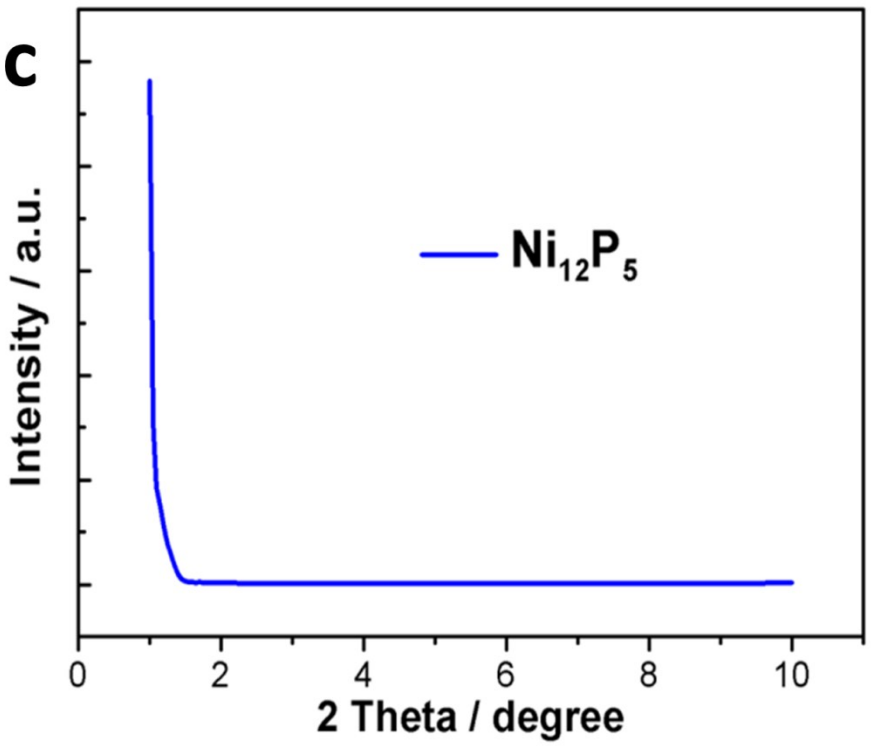
c
Intensity / a.u.
Ni12P5
0
2
4
6
8
10
2 Theta / degree

Fig. S2 SEM image (a), TEM image (b), N_2 adsorption-desorption isotherms (c) and BJH pore-size distribution (d) of as-prepared $Ni_{12}P_5$ solid spheres.

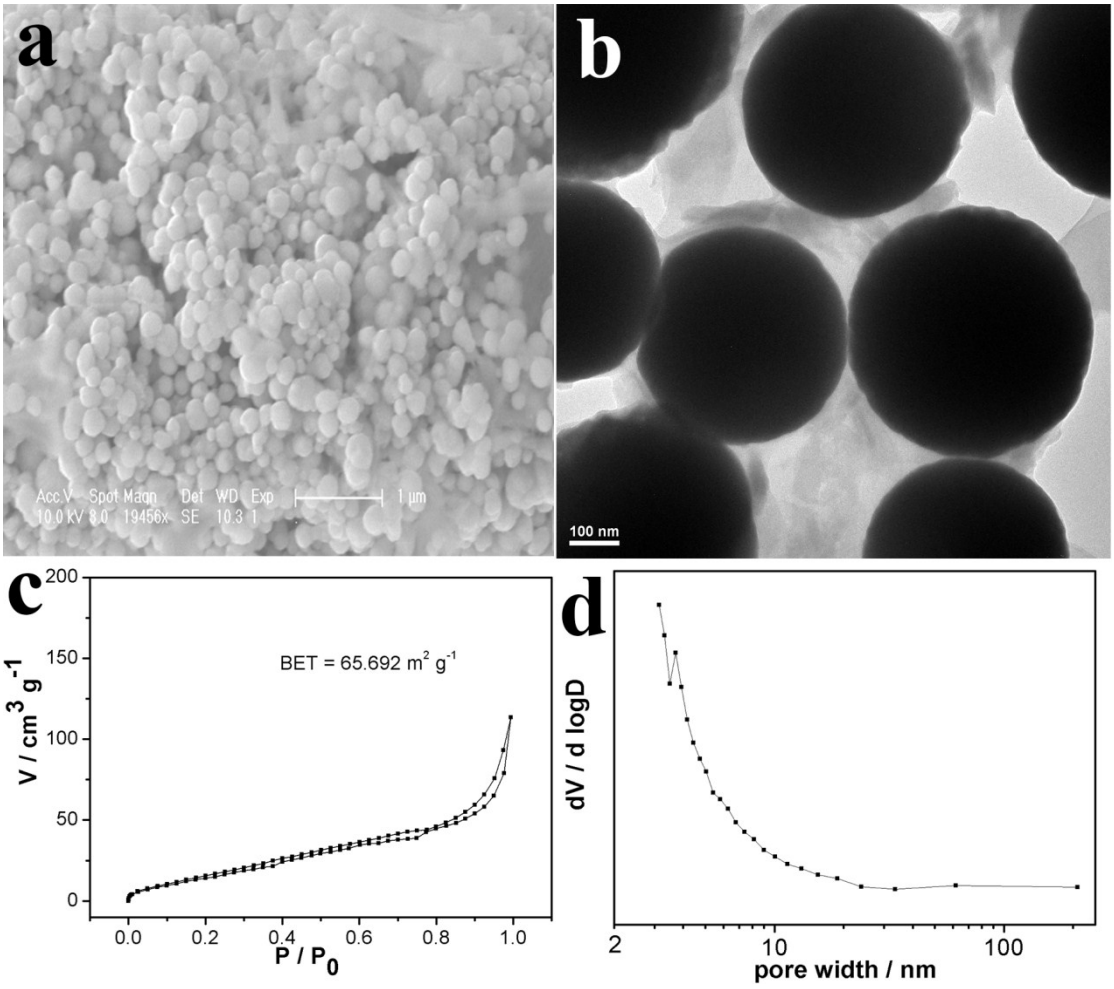

Fig. S3 mass effect of $Ni_{12}P_5$ hollow spheres. Polarization curves without (a) and without (b) iR-correction.

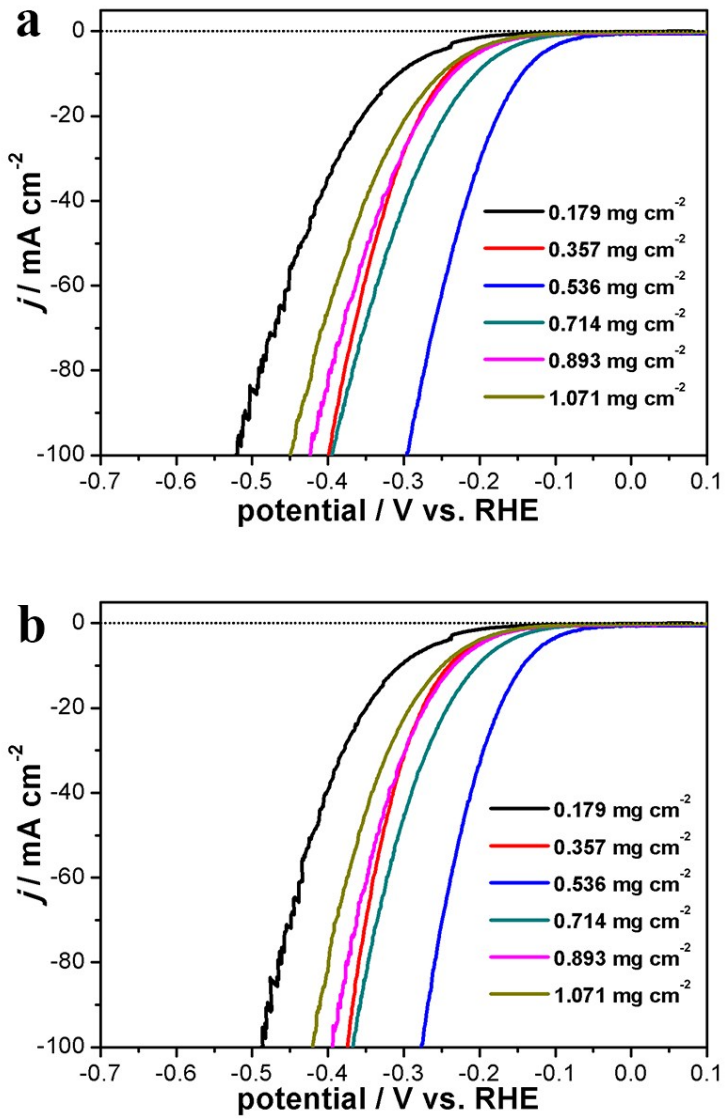

Figure S4 Nyquist plots of $Ni_{12}P_5$ solid spheres and $Ni_{12}P_5$ hollow spheres at an overpotential of 50 mV.

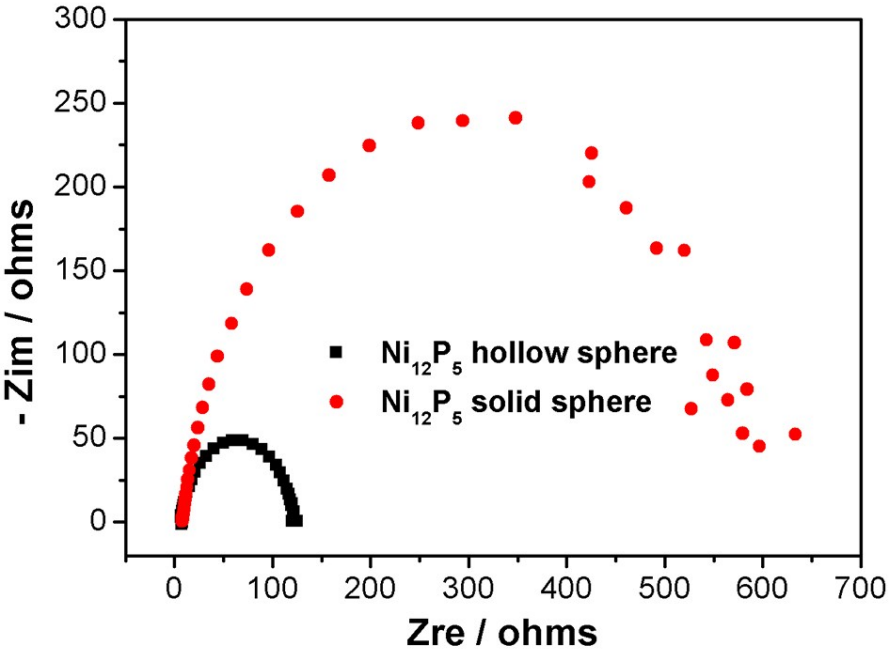

Fig. S5 Calculated versus actual hydrogen production catalyzed by $Ni_{12}P_5$ hollow spheres at a constant current of 10 mA cm^{-2} in 0.5 M H_2SO_4.

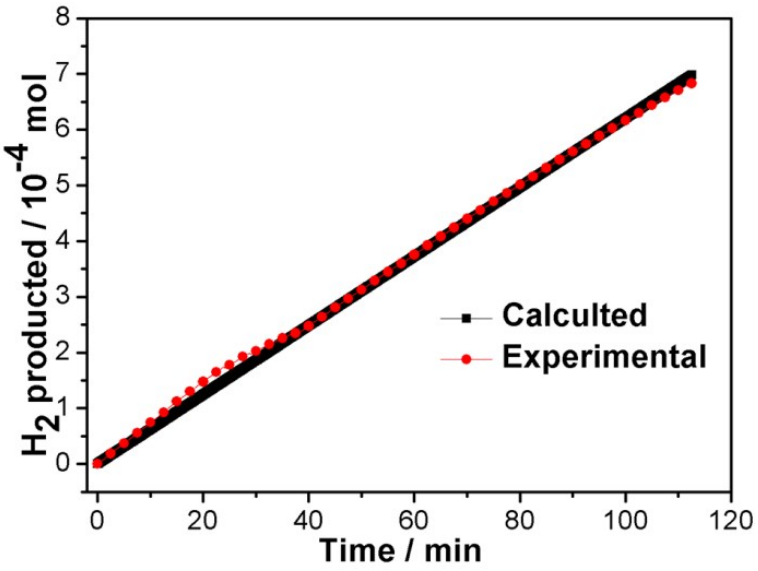

Video. A short video about the hydrogen produced under η = -200 mV.

References

1. E. J. Popczun, J. R. McKone, C. G. Read, A. J. Biacchi, A. M. Wiltrout, N. S. Lewis and R. E. Schaak, *J. Am. Chem. Soc.*, 2013, **135**, 9267-9270.
2. L. Feng, H. Vrubel, M. Bensimon and X. Hu, *Phys. Chem. Chem. Phys.*, 2014, **16**, 5917-5921.
3. Z. Huang, Z. Chen, Z. Chen, C. Lv, H. Meng and C. Zhang, *ACS Nano*, 2014, **8**, 8121-8129.
4. P. Jiang, Q. Liu and X. Sun, *Nanoscale*, 2014, **6**, 13440-13445.
5. Z. Jin, P. Li, X. Huang, G. Zeng, Y. Jin, B. Zheng and D. Xiao, *J. Mater. Chem. A*, 2014, **2**, 18593-18599.
6. Z. Pu, Q. Liu, C. Tang, A. M. Asiri and X. Sun, *Nanoscale*, 2014, **6**, 11031-11034.
7. Y. Bai, H. Zhang, L. Fang, L. Liu, H. Qiu and Y. Wang, *J. Mater. Chem. A*, 2015, **3**, 5434-5441.
8. Y. Bai, H. Zhang, X. Li, L. Liu, H. Xu, H. Qiu and Y. Wang, *Nanoscale*, 2015, **7**, 1446-1453.
9. Z.-x. Cai, X.-h. Song, Y.-r. Wang and X. Chen, *ChemElectroChem*, 2015, **2**, 1665-1671.
10. Y. Feng, Y. OuYang, L. Peng, H. Qiu, H. Wang and Y. Wang, *J. Mater. Chem. A*, 2015, **3**, 9587-9594.
11. A. Han, S. Jin, H. Chen, H. Ji, Z. Sun and P. Du, *J. Mater. Chem. A*, 2015, **3**, 1941-1946.
12. J. L. Lado, X. Wang, E. Paz, E. Carbó-Argibay, N. Guldris, C. Rodríguez-Abreu, L. Liu, K. Kovnir and Y. V. Kolen'ko, *ACS Catalysis*, 2015, **5**, 6503-6508.
13. A. B. Laursen, K. R. Patraju, M. J. Whitaker, M. Retuerto, T. Sarkar, N. Yao, K. V. Ramanujachary, M. Greenblatt and G. C. Dismukes, *Energy Environ. Sci.*, 2015, **8**, 1027-1034.
14. H. Li, W. Wang, Z. Gong, Y. Yu, l. Piao, H. Chen and J. Xia, *J. Phys. Chem. Solids*, 2015, **80**, 22-25.
15. J.-S. Moon, J.-H. Jang, E.-G. Kim, Y.-H. Chung, S. J. Yoo and Y.-K. Lee, *Journal of Catalysis*, 2015, **326**, 92-99.
16. Y. Pan, W. Hu, D. Liu, Y. Liu and C. Liu, *J. Mater. Chem. A*, 2015, **3**, 13087-13094.